Appl. Phys. B 87, 29–36 (2007)
DOI: 10.1007/s00340-006-2555-9

Applied Physics B
Lasers and Optics

V.P. KANDIDOV[1]
A.E. DORMIDONOV[1]
O.G. KOSAREVA[1,✉]
N. AKOZBEK[2]
M. SCALORA[3]
S.L. CHIN[4]

Optimum small-scale management of random beam perturbations in a femtosecond laser pulse

[1] International Laser Center, Physics Department, M.V. Lomonosov Moscow State University, Moscow 119992, Russia
[2] Time Domain Corporation, Cummings Research Park, 7057 Old Madison Pike, Huntsville, AL 35806, USA
[3] Charles M. Bowden Research Center, AMSRD-AMR-WS-ST, RDECOM, Redstone Arsenal, AL 35898-5000, USA
[4] Centre d'Optique, Photonique et Laser (COPL) et Département de Physique, de Génie Physique et d'Optique, Université Laval, Québec, QC, G1K 7P4 Canada

Received: 12 October 2006
Published online: 23 January 2007 •

ABSTRACT We have performed statistical simulations of stochastic filament control in a femtosecond laser pulse. Suppression of random multiple filaments is performed by means of a mesh introduced into the transverse beam section at the laser system output. The optimum size of a single square mesh unit contains (3.1-3.2) P_{cr} for self-focusing in the medium. Controlled filaments are formed in several groups along the laser pulse propagation direction. Almost simultaneous formation of multiple filaments can be attained by means of spatial modulation of the mesh transmission coefficient.

PACS 42.65.Jx; 42.79.Gn

1 Introduction

The phenomenon of femtosecond laser pulse energy localization in the course of filamentation is attractive for many applications. Structural modification of transparent dielectric solids is the basis for the fabrication of micro-optics devices, such as waveguides [1–3], diffraction gratings [4, 5], photonic crystals [6, 7]. Fabrication of such devices require precise localization of femtosecond pulse energy deposition within the bulk of optical material.

In femtosecond laser pulse amplification systems used for atmospheric sensing applications, the peak power of the pulse is many times higher than the critical power for self-focusing in air [8]. The initial laser pulse breaks up into multiple filaments distributed chaotically in the direction perpendicular to the laser pulse propagation. This is due to the modulational instability of the light field in the conditions of self-focusing [9]. Multiple filaments originate from both imperfections of the beam profile at the laser system output [10] as well as random fluctuations of the refractive index in the medium [11]. Stochastic nature of multiple filamentation is the reason for the instability of the backscattered nonlinear fluorescence signal obtained using the lidar measurements on the propagation path in air [12]. Progress in femtosecond laser technologies in both micro-optics and atmospheric optics offers a challenge in developing the methods for the suppression of random multiple filamentation in the bulk of transparent media.

The possibility to organize several random filaments in air by imposing either strong field gradients or phase distortions in the initial beam profile of an intense femtosecond laser pulse has been shown in [13]. The authors of [13] study both experimentally and numerically formation of the regular filamentation patterns due to the introduction of trefoil mask, circular diaphragm or forcing astigmatism in the initial beam. Detailed experiments on controlling multifilamentation by means of large-scale changes of the beam intensity and phase have been performed in [14, 15]. The authors of [14] experimentally demonstrate that elliptic distribution of the field intensity stabilizes the positions of multiple filaments in the beam in spite of the initial noise. Squeezing the whole beam with the preservation of its random structure leads to at least three order of magnitude increase in the laser plasma induced nonlinear fluorescence signal registered in the course of filamentation in air [15].

Multiple filament control by means of regular small-scale modulation of the light field in the transverse beam section has been suggested in [16–18]. The introduction of spatial phase modulation by means of a microlens array or mirror consisting of microelements leads to successful suppression of atmospheric turbulence in air and formation of the robust bunch of filaments. Periodic intensity modulation introduced by means of a wire mesh eliminates the effect of random intensity fluctuations in the initial beam profile on multiple filament formation [16, 17]. It is shown both experimentally and numerically that the periodic mesh initiates multiple filaments with almost deterministic spatial positions in the presence of additive noise with the amplitude of 10% relative to the peak light field amplitude. Numerical simulations were performed in the plane wave approximation, which is valid in the case of the large excess of the initial beam diameter over the mesh period.

In this paper, we present the results of optimizing the mesh parameters to increase the effectiveness of random light field fluctuation suppression in the beam with the transverse intensity distribution similar to the one obtained at the output of a terawatt Ti:sapphire laser system. Elaboration of the opti-

✉ Fax: +7(495) 939-3113, E-mail: kosareva@phys.msu.ru

mum relation between the mesh geometry and initial pulse energy is of crucial importance for both waveguide writing and atmospheric remote sensing applications.

2 Model of multiple filament formation in the presence of a mesh wire

Formation of filaments in a femtosecond laser pulse is the result of the combined effect of diffraction, material dispersion, self-focusing due to the Kerr nonlinearity as well as refraction on the laser-produced plasma [19]. Because of the selective nature of the Kerr-induced self-focusing towards the power, the central part of the pulse is affected first. The peak intensity is growing up to the photoionization threshold. After the ionization threshold is reached, the plasma accumulates with time. This plasma mostly affects the trailing part of the pulse, where the aberrational transverse rings are created. Further in the propagation the pulse experiences material dispersion, delayed Kerr response, and self-steepening [20, 21]. As a result, a complicated spatio-temporal intensity distribution is formed. This distribution contains a high-intensity core with 3%–12% of the total pulse energy contained in it [22]. This core with the accompanying plasma is typically called a filament.

Nonstationary transformation of a femtosecond laser pulse in the course of filamentation is described in the slowly varying envelope approximation. The equation for the light field complex amplitude $E(x, y, z, t)$ in the retarded coordinate system ($\tau = t - z/v_g$) is given by:

$$2ik\frac{\partial E}{\partial z} = \Delta_\perp E - kk_\omega''\frac{\partial^2 E}{\partial \tau^2} + \frac{2k^2}{n_0}\Delta n(x, y, z, \tau)E - ik\alpha E\,, \tag{1}$$

where $\Delta_\perp = \partial^2/\partial x^2 + \partial^2/\partial y^2$, $k = \frac{2\pi}{\lambda}n_0$ is a wavenumber, n_0 is the linear refractive index of the medium, and v_g is the group velocity of the pulse. The first term on the right-hand side of (1) describes the diffraction, the second term describes the group velocity dispersion, the third term and the fourth terms are responsible for the nonlinear refraction and the ionization loss, respectively.

The nonlinear contribution to the refractive index Δn originates from both Kerr and plasma nonlinearities and takes the form:

$$\Delta n = \Delta n_k + \Delta n_p\,. \tag{2}$$

where the Kerr nonlinear contribution is given by:

$$\Delta n_k = 0.5 n_{2\mathrm{eff}}|E|^2\,. \tag{3}$$

The simulations are performed in the conditions of a 42 fs pulse propagating in the cell filled with liquid methanol. Therefore, the effective Kerr nonlinear coefficient $n_{2\mathrm{eff}}$ is defined through the experimentally obtained critical power for self-focusing in the cell: $n_{2\mathrm{eff}} = \frac{3.77\lambda^2}{8\pi n_0 P_{\mathrm{crit}}} \approx 10^{-16}\ \mathrm{cm^2\,W}$. The critical power $P_{\mathrm{cr}} = 8$ MW for almost the same pulse duration (38 fs) was obtained in [23]. Introduction of the effective value $n_{2\mathrm{eff}}$, similarly to what was done in [10], allows us to take into account both instantaneous and delayed nonlinear response of methanol.

The nonlinear contribution Δn_p from the laser-produced plasma is defined by the quasi-free electron density N_e which is calculated according to the kinetic equation for the ionization in liquid [23].

Random fluctuations of the complex light field amplitude at the laser system output are represented by the additive perturbations $\tilde{\xi}(x, y)$. Therefore the complex amplitude of a Gaussian pulse with Gaussian transverse intensity distribution can be represented by the following expression:

$$\tilde{E}_i(x, y, z = 0, \tau) = E_0(1 + \tilde{\xi}_i(x, y))\exp\left(-\frac{x^2 + y^2}{2a_0^2} - \frac{\tau^2}{\tau_0^2}\right)C_i\,, \tag{4}$$

where a_0 and τ_0 are the initial beam radius and the half pulse duration at e^{-1} intensity level, E_0 is the amplitude of the pulse light field without the intensity fluctuations. One random realization given by (4) corresponds to a single-shot pulse at the laser system output.

The random function obeys the normal distribution law with zero mean value and the variance σ^2. The spatial correlation of the perturbations in the transverse section is given by the Gaussian correlation function:

$$B(x, y) = \sigma^2\exp\left(-\frac{x^2 + y^2}{R_{\mathrm{cor}}^2}\right)\,. \tag{5}$$

The correlation radius R_{cor} was chosen so that the peak power $P_{R_{\mathrm{cor}}}$ contained in the perturbation with this radius exceeds the critical power for self-focusing P_{cr} on the condition that this perturbation is located near the beam axis and its peak intensity is equal to the pulse peak intensity $I_0 = \frac{cn_0}{8\pi}|E_0|^2$:

$$P_{R_{\mathrm{cor}}} \geq P_{\mathrm{cr}}\,, \tag{6}$$

$$\text{where}\, P_{R_{\mathrm{cor}}} = \pi R_{\mathrm{cor}}^2 I_0\,. \tag{7}$$

According to [9], the perturbation with the size R_{cor} has the fastest instability growth rate if $P_{R_{\mathrm{cor}}} = P_{\mathrm{cr}}$. Thus, we create favorable conditions for the development of stochastic filamentation.

The normalizing factor C_i for each random realization of the light field $\tilde{E}_i$ is defined from the condition that the power of the radiation $\tilde{P}_{\mathrm{peak}}$ contained in the transverse beam section should remain a constant value from one random realization to another or from one laser shot to another:

$$\tilde{P}_{\mathrm{peak}} = P_{\mathrm{peak}}\,, \tag{8}$$

where

$$\tilde{P}_{\mathrm{peak}} = \frac{cn_0}{8\pi}\int\int\left|\tilde{E}_i(x, y, z = 0, \tau = 0)\right|^2 \mathrm{d}x\mathrm{d}y\,,$$
$$P_{\mathrm{peak}} = \pi a_0^2 I_0\,. \tag{9}$$

Substituting $\tilde{E}_i$ from (4) into (9) and (8), we have

$$C_i^2 = \frac{\pi a_0^2}{\int\int\left|1 + \tilde{\xi}_i(x, y)\right|^2\exp\left(-\frac{x^2+y^2}{a_0^2}\right)\mathrm{d}x\mathrm{d}y}\,. \tag{10}$$

In this way we exclude the influence of random peak power fluctuations in different realizations corresponding to different laser shots.

Regular intensity perturbations were specified by introducing the periodic mesh with the square unit of a period d. The mesh period d was varied in a wide range of values with the purpose to find the optimum geometrical parameters of the mesh for the multiple filament control. Each mesh unit was represented by a square with the side d. The transmittance coefficient of the mesh T_{mesh} is unity within each unit and close to zero on the boundaries with the width $h \ll d$:

$$T_{\text{mesh}}(x, y) = \sum_{k,l=-N}^{N-1} \exp\left\{-\left(\frac{x-(k+1/2)d}{(d-h)/2}\right)^{2s}\right\} \times \exp\left\{-\left(\frac{y-(l+1/2)d}{(d-h)/2}\right)^{2s}\right\}, \quad (11)$$

where $s = 6$ is the degree of the supergaussian function, $2N \times 2N$ is the total number of mesh units and the aggregate (k, l) corresponds to an individual unit in the mesh. The width h of the opaque part of the mesh is small as compared to the mesh period d, so that the resulting energy loss is within 10%–20% of the initial pulse energy before the mesh.

In the simulations we compare three regimes of filamentation: the periodic multifilamentation with the initial light field distribution given by:

$$E(x, y, z = 0, \tau) = E_0 \exp\left(-\frac{x^2+y^2}{2a_0^2} - \frac{\tau^2}{\tau_0^2}\right) T_{\text{mesh}}(x, y)\,. \quad (12)$$

This regime simulates a hypothetical case corresponding to the multifilamentation of an ideal Gaussian pulse transmitted through the mesh. The second regime simulates the stochastic multifilamentation corresponding to the small-scale self-focusing of a "real" laser pulse with random spatial perturbations of the light field at the laser system output. In this case the initial light field distribution of the pulse is given by (4). The third regime is called the controlled filamentation. This regime simulates an experiment, in which a laser pulse with random spatial perturbations is transmitted through the mesh:

$$\tilde{E}_i(x, y, z = 0, \tau) = E_0\left(1 + \tilde{\xi}_i(x, y)\right) \times \exp\left(-\frac{x^2+y^2}{2a_0^2} - \frac{\tau^2}{\tau_0^2}\right) C_i T_{\text{mesh}}(x, y)\,. \quad (13)$$

The full nonstationary 3D+1 problem formulated in (1)–(5) requires large amount of computational resources. Indeed, typical mesh period in the experiment is about 400 μm, while the beam diameter is around 5 mm [17]. Thus, there are more than 100 mesh units within the beam area. Adequate description of the small-scale self-focusing in such conditions requires at least 2048×2048 computational grid points in the (x, y) domain as well as at least 1024 grid points in the temporal domain. The size of such three-dimensional array of complex values is 34 Gb and the estimated time of calculations on IBM Cluster 1350 computer being at our disposal is around 96 h per one realization.

However, the formation of filaments occurs at the initial stage of the filamentation, when the intensity increases up to the photoionization threshold of the medium. Below this threshold a spatial and temporal intensity distribution experiences the modification mainly due to the Kerr self-focusing, which defines the spatial location of filaments. Therefore, the nonlinear refraction in the laser-produced plasma and the photoionization energy loss can be neglected. Moreover, we can leave out the contribution of material dispersion and pulse self-steepening. Indeed, these processes are responsible for temporal pulse transformation and have negligible effect on the transverse dynamics of multiple filaments [24]. Thus, in order to find the optimum parameters of the mesh and the incoming radiation needed for the optimum suppression of stochastic filamentation, it is sufficient to consider multiple filament development up to the distance where the plasma generation takes place.

As a result, we reduce the full problem to a stationary small-scale self-focusing of a Gaussian beam. The power of the beam P coincides with the peak power P_{peak} (9) of a femtosecond laser pulse, which defines the starting location of filamentation. In accordance with the accepted approximation, the equation for the complex amplitude of the light field $E(x, y, z)$ has the form:

$$2ik\frac{\partial E(x, y, z)}{\partial z} = \frac{\partial^2 E}{\partial x^2} + \frac{\partial^2 E}{\partial y^2} + \frac{2k^2}{n_0} n_2 |E|^2 E(x, y, z)\,. \quad (14)$$

In this equation we consider the propagation of the central slice of the pulse ($\tau = 0$) until the peak intensity reaches the threshold intensity for the ionization in the medium. In liquid methanol this threshold intensity is about 10^{13} W/cm^2 [23].

In this paper we discuss the control of stochastic multifilamentation in a cell with liquid. However, the same principle of introducing the periodic intensity or phase perturbations can be applied for governing the propagation in gases, including atmospheric air. Therefore, it is useful to introduce the similarity criteria of the problem, which help to apply the developed technique to multifilamentation in various optical media. As the critical power for self-focusing we will use the value P_{cr} for the Gaussian pulse [25]:

$$P_{\text{cr}} = 3.77\frac{\pi n_0}{2k^2 n_2}\,. \quad (15)$$

The most important parameters are (i) the ratio between the pulse peak power P_{peak} defined by (9) and the critical power P_{cr}, $P_{\text{peak}}/P_{\text{cr}}$; (ii) the ratio between the peak power $P_{\text{unit}} = d^2 I_0$ contained in the near-axis single mesh unit with the size d and the critical power P_{cr}, $\mathrm{P}_{\text{unit}}/P_{\text{cr}}$; (iii) the ratio between the peak power $P_{R_{\text{cor}}}$ contained in a random perturbation with the radius R_{cor} (see (7)) and the critical power P_{cr}, $P_{R_{\text{cor}}}/P_{\text{cr}}$. Additionally, when applying the mesh technique for multiple filament control, it is necessary to be aware of the variance σ^2 of the initial spatial fluctuations $\tilde{\xi}(x, y)$ (see (4) and (5)) and the ratio between the width h of the opaque part of the mesh and the period d.

The simulations were performed on the transverse grid with nonequidistant grid step size [26]. The overall size of the transverse region was $6a_0 \times 6a_0$, while the central region with

equidistant grid steps was $2a_0 \times 2a_0$. The grid step size in the latter region was $0.001a_0$, which allows us to reproduce adequately small-scale filamentation in the high-intensity zone of the beam. In the outer region with $|x|, |y| > a_0$ the grid steps Δx, Δy gradually increase according to the equation $\Delta x_{m+1} = \Delta x_m(1+\varepsilon)$, $\Delta y_{m+1} = \Delta y_m(1+\varepsilon)$, where $\varepsilon = 0.01$. In total, the computational grid in the transverse plane of the pulse contains about 3000×3000 units, with high spatial resolution ($a_0/\Delta x \approx 10^3$) in the paraxial area of the beam.

We consider multiple filament control in the conditions close to the experiment [17]. The femtosecond pulse with the duration 42 fs FWHM ($\tau_0 = 25$ fs) centered at 800 nm with the energy 130 μJ and the radius $a_0 = 2.4$ mm was transmitted through the mesh with the period $d = 0.2a_0$ and opaque part $h \approx 0.016a_0$. Immediately after the mesh we "place" an infinite cell with methanol, where multiple filaments are generated. The ratio of the pulse peak power to the critical power for self-focusing in methanol is $P_{\text{peak}}/P_{\text{cr}} = 370$, and the peak intensity is $I_0 \approx 1.6 \times 10^{10}$ Wcm^2. For the filament formation distance we assume the distance where the intensity reaches the value of $\approx 10^{13}$ W/cm^2. Here the calculations are terminated, since the stationary model breaks down for larger distances.

3 Controlled multiple filaments

In order to analyze different regimes of filamentation, we consider the intensity distribution in the transverse plane perpendicular to the pulse propagation direction. The upper row of Fig. 1a–c, shows the transverse intensity profile at the entrance to the methanol cell ($z = 0$). In the lower row of Fig. 1d–f, there is the transverse intensity distribution at a distance, where the maximum intensity almost reaches the ionization threshold ($I_{\max} \approx 300 I_0$).

Each column of Fig. 1 corresponds to the different regime of multifilamentation. In the left column (Fig. 1a and d) one can see the development of periodic, purely regular filaments, from the initial light field given by the (12), where $\tau = 0$. The column in the middle (Fig. 1b and e) shows the formation of stochastic filaments, with the initial amplitude given by the (5), where $\tau = 0$. Finally, the right column (Fig. 1c and f) demonstrates the regime of controlled filamentation, when the initially random beam is transmitted through the mesh. The initial light field amplitude is given by (13), where $\tau = 0$.

For the purpose of comparison, random fluctuations of the light field introduced by the function $\tilde{\xi}(x, y)$ are exactly the same in the regime of controlled filamentation (Fig. 1c, f) and in the regime of stochastic filamentation (Fig. 1b, e). The variance of the random function is , and the energy parameters are: $P_{\text{peak}}/P_{\text{cr}} = 370$, $P_{\text{unit}}/P_{\text{cr}} = 3.7$, $P_{R_{\text{cor}}}/P_{\text{cr}} = 1.5$. The latter ratio of $P_{R_{\text{cor}}}/P_{\text{cr}} = 1.5$ means that we create favorable conditions for stochastic filament development from the random noise $\tilde{\xi}(x, y)$ [9].

In the periodic regime shown in Fig. 1d there are 12 regular filaments formed at a distance $z = 15$ cm ($0.0025ka_0^2$). In the stochastic regime (Fig. 1e) only three filaments are formed by $z = 18$ cm ($0.0030ka_0^2$). Control of these stochastic perturbations by means of the mesh leads to the intensity distribution, which is much closer to the periodic than to the stochastic case (Fig. 1d and f). Indeed, at the distance $z = 17$ cm ($0.0028ka_0^2$) the number of controlled filaments is 11 (Fig. 1f), that is close to the number of periodic filaments in Fig. 1d. We note that the largest number of filaments is formed in the periodic case; moreover, these filaments are formed closest from the laser system output (Fig. 1d). The least number of filaments is formed in the stochastic case, and these filaments are formed farthest from the laser system output (Fig. 1e).

The possibility to suppress random filamentation depends, to a large extent, on what kinds of filaments are formed closer to the laser system output: random or regular. This is illustrated in Fig. 2a and b, where successive formation of filaments with propagation distance is shown for periodic case as well as stochastic and controlled cases with different noise level σ^2.

In the periodic case (Fig. 2a, curve marked by circles) the filaments appear in groups with the distance z. The first group

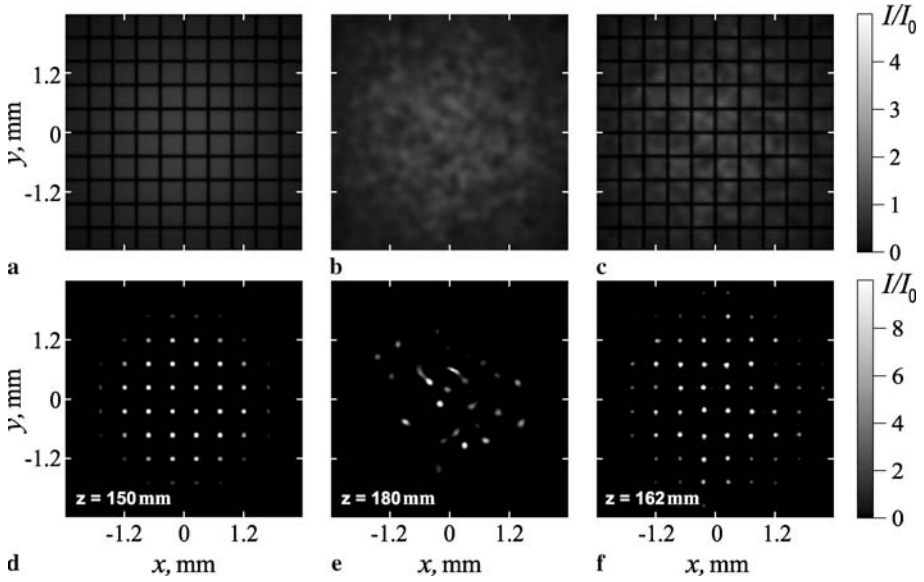

FIGURE 1 Transverse intensity distribution in the case of periodic (**a**), (**d**), stochastic (**b**), (**e**) and controlled (**c**), (**f**) filamentation. The *upper panels* (**a**)–(**c**) show the transverse intensity distribution in the central slice of the pulse $\tau = 0$ at $z = 0$, the *lower panels* (**d**)–(**f**) show multiple filaments at the distance where the most intense filament reached $300I_0$. The mesh period $d = 0.2a_0$, the ratio $P_{\text{peak}}/P_{\text{cr}} = 370$, $P_{\text{unit}}/P_{\text{cr}} = 3.7$, $P_{R_{\text{cor}}}/P_{\text{cr}} = 1.5$, the variance of the random function is in *panels* (**b**), (**c**), (**e**), (**f**)

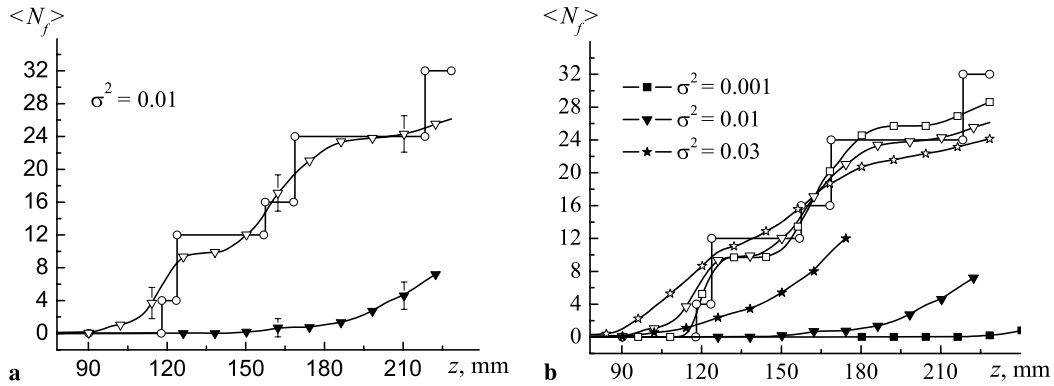

FIGURE 2 Average number of filaments as the function of the propagation distance. In both panels (**a**) and (**b**) *open circles* indicate the growth of periodic filaments without the initial noise ($\sigma^2 = 0$). The curves marked by *closed squares*, *closed triangles*, and *closed stars* indicate the growth of stochastic filaments for $\sigma^2 = 0.001$, $\sigma^2 = 0.01$ and $\sigma^2 = 0.03$, respectively. The curves marked by *open squares*, *open triangles*, and *open stars* indicate the growth of controlled filaments for $\sigma^2 = 0.001$, $\sigma^2 = 0.01$ and $\sigma^2 = 0.03$, respectively. The mesh period $d = 0.2a_0$, the ratio $P_{\text{peak}}/P_{\text{cr}} = 370$, $P_{\text{unit}}/P_{\text{cr}} = 3.7$, $P_{R\text{cor}}/P_{\text{cr}} = 1.5$

includes four filaments, which are located in the center of the four mesh units in the paraxial area of the beam. Faster development of this first group is associated with the higher peak intensity, and, hence, the peak power per a mesh unit as compared with the rest of the beam. The second group consists of 8 filaments that are formed in the eight units adjacent to the first four units. As a consequence, the total number of filaments increases to 12 at $z = 15$ cm. The next stages are associated with the development of 16 and 24 filaments. This stepwise appearance happens due to the symmetrical location of the mesh units relative to the beam center.

The average number of filaments $\langle N_{\text{f}} \rangle$ in Fig. 2 in the case of stochastic and controlled filamentation is obtained by the formation of the ensemble of 50 random statistically independent realizations of the light field $\tilde{E}_i z = 0$. Then these realizations are propagated through the medium and the average number of filaments is calculated at several z-positions. As the result, in Fig. 2a, we can see that stochastic filaments with the noise level $\sigma^2 = 0.01$ are formed later in the propagation than the periodic filaments (compare solid curve marked by circles and solid curve marked by closed triangles). Therefore, the control of these stochastic filaments with a mesh is quite effective: controlled filaments follow the same steps as the periodic filaments (compare solid curves marked by open circles and open triangles in Fig. 2a).

The increase of the noise level makes control of stochastic filamentation less effective. To demonstrate this, we plot the pairs of curves showing the growth of filaments in the stochastic and controlled cases in Fig. 2b. For each pair of curves marked by the same symbol the noise variance σ^2 is the same. Closed symbols are employed for the stochastic case and the similar open symbols indicate the corresponding case of controlled filamentation. Note the decreasing distance to the filament formation in the stochastic case as the variance σ^2 increases from $\sigma^2 = 0.001$ to $\sigma^2 = 0.03$ (see the curves marked by closed symbols in Fig. 2b). The consequence of this decrease is larger deviation of the corresponding curves indicating the growth of controlled filaments from the ideal curve for the growth of regular filaments (compare the curve marked by circles and the curves marked by open squares, triangles and stars in Fig. 2b).

4 Optimum mesh parameters

According to Fig. 2 the effective control of stochastic filaments can be performed, if we force the regular filaments to be formed earlier in the propagation than the stochastic ones. Therefore, the optimization of multiple filament control requires minimization of the distance to the formation of the regular filaments. For a fixed initial pulse peak power P_{peak}, we can vary the mesh unit size d and try to find such value, which ensures the earliest formation of the regular filaments for the given conditions. We simulate the propagation in the regime of periodic multifilamentation with different values of the ratio $P_{\text{unit}}/P_{\text{cr}}$, leaving all the other parameters of the pulse and the medium invariable.

Figure 3 shows the distance to the formation of the first burst of filaments as the function of the single unit peak power P_{unit} related to the critical power for self-focusing P_{cr}. By the first burst of filaments, we mean the four filaments born in the central mesh units (Fig. 2a, curve marked by circles). Dependence of the filament formation distance on the mesh unit power P_{unit} was performed in a wide range of maximum initial intensity $I_{\max} = 0.5$–$2I_0$ of the beam (and, consequently, the

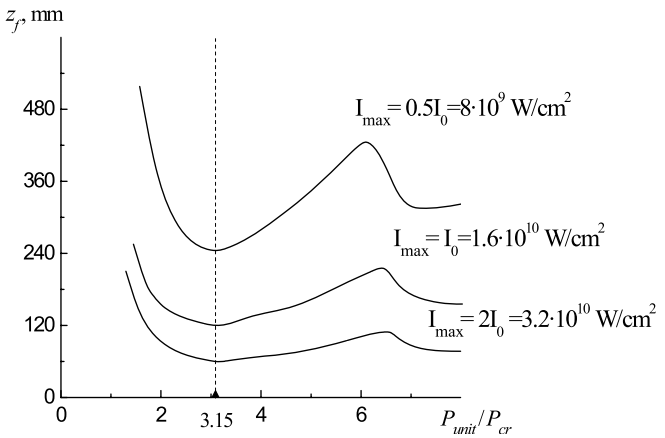

FIGURE 3 Distance z_{f} to the first filament formation in the periodic filamentation regime (no noise) as the function of the mesh unit peak power $P_{\text{unit}} \approx d^2 I_{\max}$ for several fixed initial intensities $I_{\max}$

initial whole beam peak power $P_{\text{peak}} = I_{\max}\pi a_0^2$). The curves for three chosen maximum intensity values are presented in Fig. 3. For the curve with the given maximum intensity $I_{\max}$ the variation in the single unit peak power $P_{\text{unit}} = d^2 \times I_{\max}$ was attained through the variation of the mesh period d. When comparing the filament formation distance at the same value of $P_{\text{unit}}/P_{\text{cr}}$ and the curves corresponding to the different intensity $I_{\max}$, one has to remember that the mesh period decreases as the inverse square root of $I_{\max}$ in order to keep the single unit power constant. As the ratio increases from 1 to 3.1–3.2, the distance z_{f} to the filament origin decreases. The reason for this is that almost the whole power within a unit contributes to the development of a single filament. The subsequent increase in filament formation distance is associated with the transition from a single to multiple filament regime. This means that the power per a single unit becomes high enough to feed several perturbations simultaneously. The competition for the power in the range of $3P_{\text{cr}} < P_{\text{unit}} < 6P_{\text{cr}}$ delays the filament formation [27]. In the range $P_{\text{unit}} > 6P_{\text{cr}}$ the four filaments are formed within each unit, and the distance to the first filament formation decreases due to the further increase of the unit power.

The remarkable result is that independently of the initial maximum intensity $I_{\max}$ the dependence of the distance to the first filament formation on the single unit power gives almost the same ratio $P_{\text{unit}}/P_{\text{cr}} = 3.1$–$3.2$ corresponding to the minimum distance of the formation of a single filament per a mesh unit. Similarly, independently of the initial intensity $I_{\max}$, the minimum distance of the formation of four filaments per a mesh unit starts from $P_{\text{unit}}/P_{\text{cr}} = 6$. As the optimum ratio $P_{\text{unit}}^{\text{opt}}/P_{\text{cr}}$, which provides the fastest regular filament formation, we consider the ratio

$$P_{\text{unit}}^{\text{opt}}/P_{\text{cr}} = (3.1{-}3.2) \tag{16}$$

Thus, the algorithm for the determination of the optimum mesh period in the particular experimental conditions takes the form: (i) calculation of the maximum intensity in the beam: $I_{\max} = P_{\text{peak}}/\pi a_0^2$ and (ii) calculation of the optimum mesh period as

$$P_{\text{unit}}^{\text{opt}} = d_{\text{opt}}^2 I_{\max} = (3.1{-}3.2)\,P_{\text{cr}}\,,$$
$$d_{\text{opt}} = (1.76{-}1.79)\sqrt{P_{\text{cr}}/I_{\max}}\,. \tag{17}$$

The next stage of the mesh parameter optimization is associated with finding the range of the mesh periods needed to suppress stochastic filamentation with the given correlation radius and noise level. To find the range of acceptable mesh periods, we performed statistical study of the filament starting position. In the initial distribution of the beam given by (5) at $\tau = 0$ we choose the noise variance σ^2 varying from 0.001 to 0.03 and the correlation radius R_{cor} varying from 60 μm to 360 μm. The corresponding peak power $P_{R_{\text{cor}}}$ was changed in the range $0.25{-}8\,P_{\text{cr}}$. For each combination of the noise variance σ^2 and the correlation radius R_{cor}, we propagated 50 statistically independent realizations of the initial beam. The resulting average distance to the first stochastic filament formation is shown by the solid curve in Fig. 4a and b. Note that random perturbations containing the power equal to $1.5P_{\text{cr}}$ produce the filaments closest to the cell entrance. This distance is longer ($z \approx 160$ mm, Fig. 4a) for the lower noise level of $\sigma^2 = 0.01$ and shorter ($z \approx 107$ mm, Fig. 4b) for the higher noise level of $\sigma^2 = 0.03$. The corresponding radius of correlation $R_{\text{cor}} = 150$ μm.

In order to define the range of the mesh periods capable to suppress random filaments, we superimpose the dependence of the filamentation distance on a single unit power in the periodic case (dashed curves in Fig. 4a and b) over the dependence of the average distance of stochastic filamentation on the power contained in the typical perturbation (solid curves in Fig. 4 a and b). In Fig. 4a there exists the range of single mesh unit powers P_{unit}, for which stochastic filaments are born later in the propagation than the periodic ones. By the example we choose the correlation radius $R_{\text{cor}} = 250$ μm. The first filament is formed at a distance $z \approx 174$ mm (filled circle in Fig. 4a). If mesh-induced periodic filaments are formed earlier in the propagation, then they can suppress stochastic filamentation with $R_{\text{cor}} = 250$ μm and $\sigma^2 = 0.01$. The corresponding range of peak powers per a mesh unit is

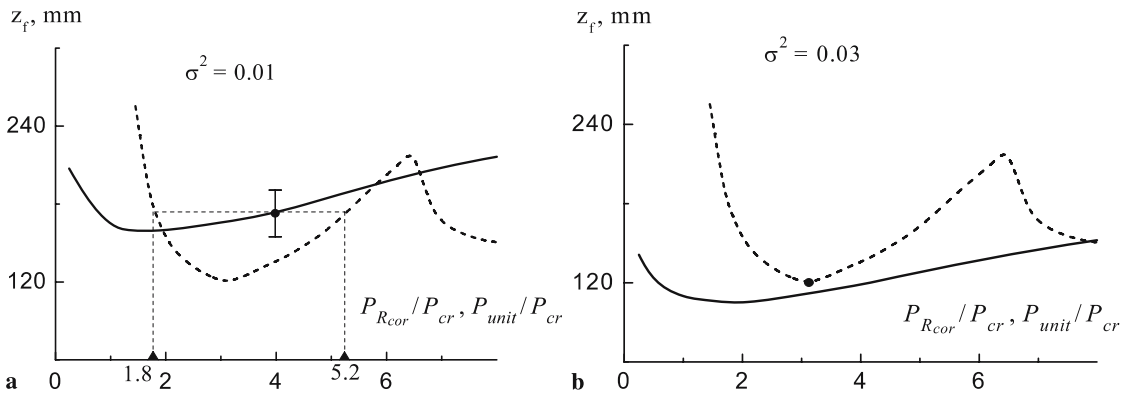

FIGURE 4 Average distance z_{f} to the formation of the first stochastic filament as the function of the ratio $P_{R_{\text{cor}}}/P_{\text{cr}}$ (*solid curves* in both panels **a** and **b**). The variance of random fluctuations is $\sigma^2 = 0.01$ (**a**) and $\sigma^2 = 0.03$ (**b**). The filament formation distance in the periodic case as the function of the ratio $P_{\text{unit}}/P_{\text{cr}}$ (*dashed curves* in both panels **a** and **b**). In panel (**a**) the *filled circle* indicates the first filament formation distance in the case of the characteristic perturbation size $R_{\text{cor}} = 250$ μm. In panel (**b**) the *filled circle* indicates the minimum distance to the periodic filament formation. *Filled triangles* in panel (**a**) indicate the range of the mesh unit power, where stochastic filamentation is suppressed successfully. The maximum intensity is $I_{\max} = I_0 = 1.6 \times 10^{10}$ W/cm^2 for all curves

$1.8P_{cr} < P_{unit} < 5.2P_{cr}$ (see the intersection of the horizontal dashed line and dashed curve in Fig. 4a).

With the increase in the initial fluctuation variance up to $\sigma^2 = 0.03$, stochastic filaments are formed earlier in the propagation than the periodic ones (Fig. 4b). This may be seen from the comparison between the minimum filamentation distance in the periodic case (filled circle in Fig. 4b) and the dashed curve showing stochastic filamentation in Fig. 4b.

Thus, depending on the initial light field fluctuation variance and the radius of correlation, the mesh can work as a very efficient tool for multiple filament control. The necessary condition is the correct choice of the mesh period in order to provide the optimum amount of power flowing through a single unit. We note that the typical variance of random fluctuations in a terawatt peak power pulse produced by the Ti:sapphire laser amplification system installed in Laval University is of the order of $\sigma^2 = 0.003$ (see, e.g., [28]). Therefore, the mesh can be used for the suppression of random filamentation in both air and condensed matter.

Fine management of the beam wavefront can be performed based on the spatial modulation of the transmission coefficient of the mesh. For the purpose of microoptics device fabrication it might be necessary to initiate the simultaneous formation of multiple filaments in the propagation direction. One way to implement this task is to delay the fast formation of the first four and then twelve filaments as it is seen in Fig. 2a (the curves marked by the open circles and triangles). To smooth this stepwise formation of filaments, we introduce partially transparent boundaries of the central mesh units. In such a way we make possible the energy flow between the neighboring units, initiate the competition between the corresponding filaments and, as a consequence, delay the intensity growth in the beam center. As the result, the perturbations growing from the periphery units catch up with the ones from the central units. One suggested way to make possible such spatially modulated transmission in the experiment is to use a glass substrate with coating in the form of a mesh. This coating may have different reflection coefficient depending on the mesh unit location relative to the beam center.

The modified transmission coefficient $T^{mod}_{mesh}(x, y)$ can be written in the form:

$$T^{mod}_{mesh}(x, y) = T_{mesh}(x, y) + (1 - T_{mesh}(x, y))A_{mod} \exp\left\{-\left(\frac{x^2+y^2}{R^2_{mod}}\right)^p\right\}, \quad (18)$$

where $0 \le A_{mod} \le 1$ is the amplitude of modulation, R_{mod} is the radius of modulation and p is the degree of the supergaussian function.

By increasing the amplitude A_{mod} and adjusting the radius R_{mod}, we can delay the filament formation in the near-axis part of the beam. As the amplitude A_{mod} reaches 0.38 and the area of the modulation spreads out to almost four central mesh units ($R_{mod} = 1.8d$), the first 16 filaments appear together in one group at a distance $z \approx 160$ mm (Fig. 5, solid curve marked by open circles). This is in contrast with the case shown in Fig. 2a, where 16 filaments are formed in three steps starting from $z \approx 120$ mm and up to $z \approx 160$ mm (Fig. 2a, solid curve marked by open circles).

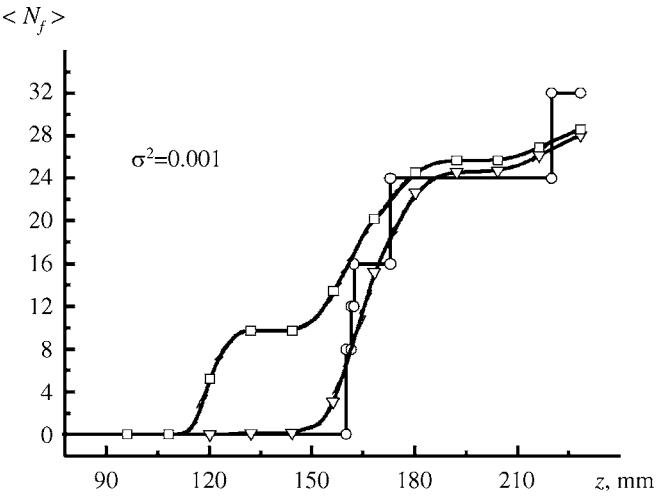

FIGURE 5 Average number of filaments as the function of the propagation distance z. *Circles* indicate the growth of regular filaments ($\sigma^2 = 0$) induced by the mesh with modulated transmission given by (18), where $R_{mod} = 1.8d$, $A_{mod} = 0.38$, $p = 2$. *Triangles* indicate the growth of controlled filaments for $\sigma^2 = 0.001$. For comparison, *open squares* show the growth of controlled filaments without modulation of the transmission ($A_{mod} = 0$). The maximum intensity is $I_{max} = I_0 = 1.6 \times 10^{10}$ W/cm^2 for all curves

When a stochastic beam is controlled by the mesh with modulated transmission, the first 16 filaments appear almost simultaneously within the region $z = 150$–165 mm (the solid curve marked by crossed squares). For comparison we plot the curve marked by open squares, which shows the stepwise filamentation of the initially stochastic beam after the ordinary mesh (no modulation of the transmission, i.e., $A_{mod} = 0$).

5 Conclusions

We have studied numerically optimization of the mesh wire parameters used for stochastic filament control in a femtosecond laser pulse propagating in the nonlinear Kerr medium. Optimization was based on the comparison of the three propagation regimes: (i) the stochastic regime corresponding to multiple filament formation from random light field perturbations; (ii) the periodic regime corresponding to mesh-induced filament formation from the ideal Gaussian pulse; (iii) the controlled regime corresponding to the filament formation in the stochastic pulse transmitted through the mesh.

Statistical processing performed over 50 random realizations of the initial noisy beam has revealed that if the variance of initial intensity fluctuations is $\sigma^2 = 0.01$ or lower, stochastic filamentation can be suppressed well by the mesh-induced perturbations. We note here that the typical variance in a terawatt peak power pulse at the output of Ti: sapphire laser amplification system is $\sigma^2 \le 0.003$. In the controlled regime the filaments produced by the pulse with the variance of perturbations $\sigma^2 \le 0.01$ appear in groups, similar to the case of periodic multifilamentation. With increasing noise in the initial beam ($\sigma^2 \ge 0.03$), stochastic formation of filaments takes place.

The most effective control is performed by the mesh, which provides the closest formation of filaments from the laser system output. By varying the peak power in a sin-

gle mesh unit, we have found that the optimum mesh period satisfying this requirement is $d_{\mathrm{opt}} = (1.76{-}1.79)\sqrt{P_{\mathrm{cr}}/I_{\mathrm{max}}}$, where I_{max} is the maximum intensity of a femtosecond pulse: $I_{\mathrm{max}} = P_{\mathrm{peak}}/\pi a_0^2$.

Fine management of the beam wavefront can be performed based on the spatial modulation of the transmission coefficient of the mesh. Increase in the transmission of the mesh boundaries in the central part of the beam leads to the simultaneous formation 12 to 16 filaments in the propagation direction.

The suggested method of the mesh parameter optimization can be used in femtosecond remote sensing applications as well as for microoptics device fabrication using ultrashort laser pulses.

ACKNOWLEDGEMENTS A.E. Dormidonov, V.P. Kandidov, O.G. Kosareva thank the support of European Research Office of the US Army through the contract No W911NF-05-1-0553 and Russian Foundation for Basic Research through grant No. 06-02-17508-a. V.P. Kandidov, O.G. Kosareva and S.L. Chin thank the support of the NATO Linkage (Grant No.PST.CLG. 980383).

REFERENCES

1 K.M. Davis, K. Miura, N. Sugimoto, K. Hirao, Opt. Lett. **21**, 1729 (1996)
2 W. Watanabe, T. Asano, K. Yamada, K. Itoh, J. Nishii, Opt. Lett. **28**, 2492 (2003)
3 A. Saliminia, N.T. Nguyen, M.C. Nadeau, S. Petit, S.L. Chin, R. Vallee, J. Appl. Phys. **93**, 3724 (2003)
4 E. Fertein, C. Przygodzki, H. Delbarre, A. Hidayat, M. Douay, P. Niay, Appl. Opt. **40**, 3506 (2001)
5 K. Yamada, W. Watanabe, K. Kintaka, J. Nishii, K. Itoh, Japan. J. Appl. Phys. **42**, 6916 (2003)
6 Y. Xu, S. Juodkazis, K. Sun, M. Wabe, S. Matsuo, H. Misawa, J. Nishii, Opt. Lett. **26**, 325 (2001)
7 R.S. Taylor, C. Hnatovsky, E. Simova, D.M. Rayner, V.R. Bhardwaj, P.B. Corkum, Opt. Lett. **28**, 1043 (2003)
8 J. Kasparian, M. Rodrigues, G. Mejean, J. Yu, E. Salmon, H. Wille, R. Bourayou, S. Frey, Y.B. Andre, A. Mysyrowicz, R. Sauerbrey, J.P. Wolf, L. Woste, Science **301**, 61 (2003)
9 V.I. Bespalov, V.I. Talanov, JETP Lett. **3**, 307 (1966)
10 S.L. Chin, S. Petit, W. Liu, A. Iwasaki, M.C. Nadeau, V.P. Kandidov, O.G. Kosareva, K.Y. Andrianov, Opt. Commun. **210**, 329 (2002)
11 S.A. Shlenov, V.P. Kandidov, Atmosph. Ocean. Opt. **17**, 565 (2004)
12 S.A. Hosseini, Q. Luo, B. Ferland, W. Liu, S.L. Chin, O.G. Kosareva, N.A. Panov, N. Akozbek, V. P Kandidov, Phys. Rev. A **70**, 033 802 (2004)
13 G. Mechain, A. Couairon, M. Franco, B. Prade, A. Mysyrowicz, Phys. Rev. Lett. **93**, 035 003-1 (2004)
14 G. Fibich, S. Eisenmann, B. Ilan, A. Zigler, Opt. Lett. **29**, 1772 (2004)
15 O.G. Kosareva, N.A. Panov, N. Akozbek, V.P. Kandidov, Q. Luo, S.A. Hosseini, W. Liu, J.F. Gravel, G. Roy, S.L. Chin, Appl. Phys. B **82**, 111 (2006)
16 H. Schroeder, J. Liu, S.L. Chin, Opt. Express **12**, 4768 (2004)
17 V.P. Kandidov, N. Akozbek, M. Scalora, O.G. Kosareva, A.V. Nyakk, Q. Luo, S.A. Hosseini, S.L. Chin, Appl. Phys. B **80**, 267 (2004)
18 N.A. Panov, O.G. Kosareva, V.P. Kandidov, N. Akozbek, Q. Luo, S.A. Hosseini, W. Liu, J. Gravel, S.L. Chin, Proc. SPIE **5708**, 91 (2005)
19 O.G. Kosareva, V.P. Kandidov, A. Brodeur, S.L. Chin, J. Nonlinear Opt. Phys. Mater. **6**, 485 (1997)
20 M. Mlejnek, E.M. Wright, J.V. Moloney, Opt. Lett. **23**, 382 (1998)
21 N. Akozbek, C.M. Bowden, S.L. Chin, J. Mod. Opt. **49**, 475 (2002)
22 V.P. Kandidov, O.G. Kosareva, A.A. Koltun, Quantum Electron. **QE-33**, 69 (2003)
23 W. Liu, S.L. Chin, O. Kosareva, I.S. Golubtsov, V.P. Kandidov, Opt. Commun. **225**, 193 (2003)
24 W. Liu, O. Kosareva, I.S. Golubtsov, A. Iwasaki, A. Becker, V.P. Kandidov, S.L. Chin, Appl. Phys. B **76**, 215 (2003)
25 J.H. Marburger, Prog. Quantum. Electron. **4**, 35 (1975)
26 V.P. Kandidov, V.Yu. Fedorov, Quantum Electron. **QE-34**, 1163 (2004)
27 O.G. Kosareva, N.A. Panov, V.P. Kandidov, Atmosph. Ocean. Opt. **18**, 204 (2005)
28 Q. Luo, S.A. Hosseini, W. Liu, J.F. Gravel, O.G. Kosareva, N.A. Panov, N. Akozbek, V.P. Kandidov, G. Roy, S.L. Chin, Appl. Phys. B **80**, 35 (2005)